Steel and Composite Structures, *Vol. 31, No. 2 (2019) 201-216*
DOI: https://doi.org/10.12989/scs.2019.31.2.201

Local buckling of rectangular steel tubes filled with concrete

Ruslan Kanishchev* and Vincent Kvocak [a]

Department of Steel and Timber Structures, Institute of Structural Engineering,
Civil Engineering Faculty, Technical University of Kosice, Vysokoskolska 4, 042 00 Kosice, Slovakia

(*Received July 21, 2018, Revised January 24, 2019, Accepted March 30, 2019*)

Abstract. This scientific paper provides a theoretical, numerical and experimental analysis of local stability of axially compressed columns made of thin-walled rectangular concrete-filled steel tubes (CFSTs), with the consideration of initial geometric imperfections. The work presented introduces the theory of elastic critical stresses in local buckling of rectangular wall members under uniform compression. Moreover, a numerical calculation method for the determination of the critical stress coefficient is presented, using a differential equation for a slender wall with a variety of boundary conditions. For comparison of the results of the numerical analysis with those collected by experiments, a new model is created to study the behaviour of the composite members in question by means of the ABAQUS computational-graphical software whose principles are based on the finite element method (FEM). In modelling the analysed members, the actual boundary and loading conditions and real material properties are taken into account, obtained from the experiments and material tests on these members. Finally, the results of experiments on such members are analysed and then compared with the numerical values. In conclusion, several recommendations for the design of axially compressed composite columns made of rectangular concrete-filled thin-walled steel tubes are suggested as a result of this comparison.

Keywords: composite structures; local buckling; concrete-filled steel tubes (CFSTs); design codes; FEM analysis

1. Introduction

The application of progressive load-bearing elements in both buildings and civil engineering constructions has become necessary due to cost-saving reasons. Composite structures made by the effective combination of two materials, such as steel and concrete, are undoubtedly regarded as progressive ones, while composite columns; in particular, constitute a significant structural element in these constructions. They are widely used in the construction of tall buildings and bridges as structural elements under compression, with relatively low bending moments. One of the chief representatives of such structures is the rectangular concrete-filled steel tube. This structural member has a number of advantages to the hollow steel tube, as was demonstrated by Kanishchev (2016); however, probably the most significant one, from the static point of view, is its resistance against the loss of local and global stability, which allows the reduction in the dimensions of the section.

Nowadays, there are enough publications pertaining to the research into the behaviour of composite columns. Sakino *et al*. (2004) explored short axially compressed CFSTs with compact steel sections. Storozhenko *et al*. (2014) carried out experiments on high-strength CFST columns subjected to an eccentric load. Ellobody and Young (2006), in their research study, introduced a sufficiently accurate non-linear behavioural model (using the FEM analysis), describing the behaviour of centrically compressed circular and rectangular composite columns. Such authors as Liu *et al*. (2003), Lee (2007) and Mouli and Khelafi (2007), Uy (2008), Huang *et al*. (2008), Aslani *et al*. (2015, 2016) investigated the axial load capacity, ultimate strength, stability and ductility characteristics of rectangular concrete-filled columns using high-strength steels and concrete under axial compression. Experimental tests, which were conducted by Chen *et al*. (2018), showed the influence of a on the residual bond-slip behavior of high strength concrete-filled square steel tube after elevated temperatures. Patel *et al*. (2012) proposed a multiscale numerical model for simulating the interaction of local and global buckling behaviour of eccentrically loaded high-strength rectangular CFST slender beam-columns with large depth-to-thickness ratios. Yang and Han (2009) presented research work aimed to experimentally investigate the behaviour of rectangular concrete-filled steel tubular stub columns loaded axially on a partially stressed cross-sectional area. Ding *et al*. (2014, 2017), for example, studied the mechanical performance of stirrup-confined concrete-filled steel tubular stub columns under axial loading. Experimental tests, which were conducted by Lin *et al*. (2018) and Zhao *et al*. (2018) on circular columns, showed that the loading paths of confined concrete in CFT column are affected by the column parameters (steel strength, the unconfined concrete strength and the D/t ratio).

Lu *et al*. (2015), Kanishchev and Kvocak (2015a) stated that a high number of standards and regulations exist for the design of the elements mentioned above; for example, Eurocode 4 is applied to the design of composite structures

*Corresponding author, Ph.D.,
E-mail: ruslan.kanishchev@tuke.sk
[a] Professor, Ph.D., E-mail: vincent.kvocak@tuke.sk

http://www.techno-press.org/?journal=scs&subpage=6 ISSN: 1229-9367 (Print), 1598-6233 (Online)

made of rectangular concrete-filled steel tubes in Europe.

The fundamental disadvantage of this standard is the restriction of its application only to compact steel sections. If materials in the design of such structures are to be employed cost-effectively, there is an urgent need to investigate Class 4 hollow steel sections (compliant with Eurocode 3) filled with concrete, which are classified outside the applicability of Eurocode 4 and, as mentioned above, have not yet been adequately researched.

2. Stability of rectangular walls under compression

Some fundamental principles for the design of thin-walled sections (those that can be categorised as Class 4 according to EN 1993-1-1) were laid down by Prof. Bryan (Bryan 1891), who established procedures for the analysis of elastic critical stresses in local buckling of long rectangular wall members with simple (hinged) supports of all their edges under uniform compression. Prof. Timoshenko *et al*. (Timoshenko and Woinowsky-Krieger 1959, Timoshenko 1971) continued in the development of this theory in his works and introduced differential equations for a slender wall (see Figs. 1(a)-(b)).

Based on Kirchhoff´s theory, when internal forces exist in the wall, the resulting forces and moments in a unit wall element can be obtained. The curvature of its surface is given by

$$k_1 = \frac{\partial^2 w}{\partial x^2}, \quad k_2 = \frac{\partial^2 w}{\partial y^2}, \quad k_3 = \frac{\partial^2 w}{\partial x \partial y} \tag{1}$$

where w is the deflection of slender walls.

The bending moments M_1, M_2 and the torsional moment T are

$$M_1 = -C(k_1 + \nu k_2), \quad M_2 = C(k_2 + \nu k_1), \quad T = -C(1-\nu)k_3 \tag{2}$$

The stiffness of the wall C is

$$C = \frac{Et^3}{12(1-\nu^2)} \tag{3}$$

where E is the modulus of elasticity of the steel; t is the wall thickness; ν is the Poisson’s ratio.

Providing that the condition of equilibrium is satisfied in this structural member (see Figs. 1(a)-(b)), it holds that

$$\frac{\partial N_1}{\partial x} + \frac{\partial U_1}{\partial y} - P_1 k_1 - P_2 k_2 = 0 \tag{4}$$

$$\frac{\partial U_2}{\partial x} + \frac{\partial N_2}{\partial y} - P_1 k_3 - P_2 k_2 = 0 \tag{5}$$

$$\frac{\partial P_1}{\partial x} + \frac{\partial P_2}{\partial y} + N_1 k_1 + N_2 k_2 + (U_1 + U_2) k_3 = 0 \tag{6}$$

$$\frac{\partial T}{\partial x} + \frac{\partial M_2}{\partial y} + P_2 = 0 \tag{7}$$

$$\frac{\partial M_1}{\partial x} - \frac{\partial T}{\partial y} - P_1 = 0 \tag{8}$$

2.1 Stability of walls with peripherally pinned (hinged) ends

If the wall is subjected to an axial compressive force $N < N_{cr}$, its shape is in-plane. For $N = N_{cr,}$ the shape of the wall may stay in-plane or move out-of-plane and become concave. If the force N is further increased, the wall becomes more concave; however, if the force N differs from N_{cr} very slightly, the concave shape of the wall (or its out-of-plane displacement) in the equilibrium state is very much that of the in-plane one. That means that the values of k_1, k_2, k_3, P_1, P_2 are so small that they can be neglected.

The condition $U_2 = N_2 = 0$ can be applied to the system of Eqs. (4)-(8). When $N_1 = -N$, the Eqs. (6)-(8) can be employed to produce a differential equation for a slender wall with peripherally hinged (pinned) ends

$$C\left(\frac{\partial^4 w}{\partial x^4} + 2\frac{\partial^4 w}{\partial x^2 \partial y^2} + \frac{\partial^4 w}{\partial y^4}\right) + N\frac{\partial^2 w}{\partial x^2} = 0 \tag{9}$$

where N is the compression force.

A particular solution for this differential Eq. (9), representing the equilibrium of forces in one of the possible buckling modes of the wall is

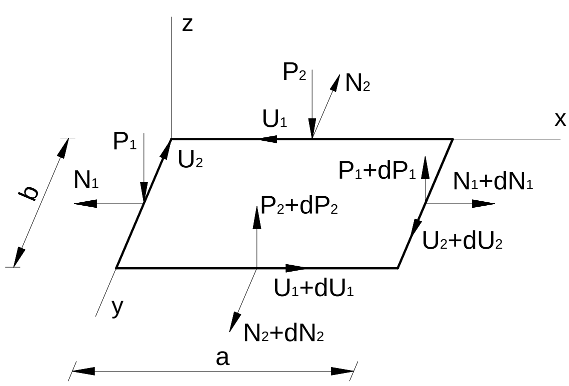

(a) Resultant forces in a unit wall element

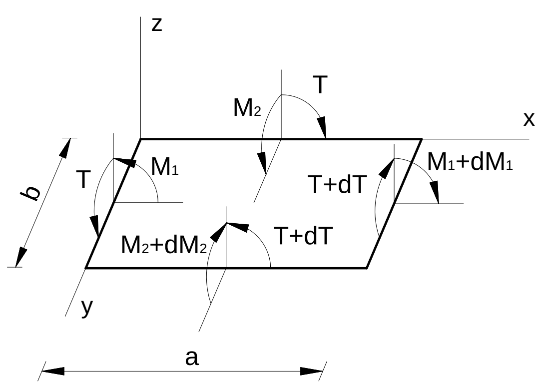

(b) Resultant bending moments in a unit wall element

Fig. 1 Mathematical model of a slender wall

$$w = A\sin\frac{m\pi x}{a}\sin\frac{n\pi y}{b} \tag{10}$$

where m and n is the half-waves of sinusoid in the direction of axis x and y.

This solutions satisfies the boundary conditions (see Figs. 1(a)-(b)) for $x = 0$ and $x = a \rightarrow w = 0$, and $M_1 = 0$, and for $y = 0$ and $y = b \rightarrow w = 0$ and $M_2 = 0$, while putting $N_1 = -N$; $U_1 = U_2 = N_2 = 0$.

If Eq. (10) is substituted into the Eq. (9)

$$N = C\pi^2\frac{\left(\frac{m^2}{a^2}+\frac{n^2}{b^2}\right)^2}{\frac{m^2}{a^2}} \tag{11}$$

It is necessary to identify such a mode of buckling of the wall out of all its possible modes in the state of equilibrium of forces in its section that the value of force N is minimal. Therefore, the right side of the Eq. (11) must be as small as possible. This obviously happens when $n = 1$. The value of m is, according to Timoshenko (1971), expressed by the Eq. (12). It can be assumed from the following equation that the ultimate length a at which the plate achieves its first buckling mode consists of m half-waves

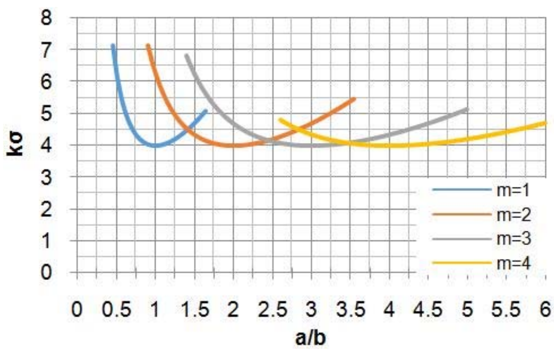

Fig. 2 Correlation between the critical stress coefficient and the length-to-width ratio of the column wall with various numbers of half-waves along its length

$$a = b\sqrt{m(m+1)} \tag{12}$$

Considering that $N/(t.b) = \sigma$, the formula (11) can be rewritten with $n = 1$, and the cylindrical stiffness of the wall can be expressed as

$$\sigma = \left(m\frac{b}{a}+\frac{1}{m}\frac{a}{b}\right)^2\frac{\pi^2 E t^2}{12(1-\nu^2)b^2} \tag{13}$$

Compliant with EN 1993-1-5, the Eq. (13) is the value of the elastic critical stress in the wall

$$\sigma_{cr} = k_\sigma\frac{\pi^2 E}{12(1-\nu^2)}\left(\frac{t}{b}\right)^2 \tag{14}$$

Fig. 2 Correlation between the critical stress coefficient and the length-to-width ratio of the column wall with various numbers of half-waves along its length

Consequently, the critical stress coefficient k_σ is given as follows (Fig. 2)

$$k_\sigma = \left(m\frac{b}{a}+\frac{1}{m}\frac{a}{b}\right)^2 \tag{15}$$

This critical stress coefficient can be used for buckling in steel section walls of a rectangular tube (Fig. 3) as the corners of the tube section may rotate due to its peripherally hinged ends.

2.2 Stability of walls with longitudinally fixed ends

If a steel tube is filled with concrete (Fig. 4), the concrete core serves as a composite member, preventing the rotation of the steel section corners, and the boundary conditions for the wall supports in the longitudinal direction change to nearly fixed ends. This change in the boundary conditions (from those with hinged ends to these with fixed ones along the unloaded longitudinal sides of the wall) requires another particular solution for the differential Eq. (9) that by Timoshenko's theory (1971) will be as follows

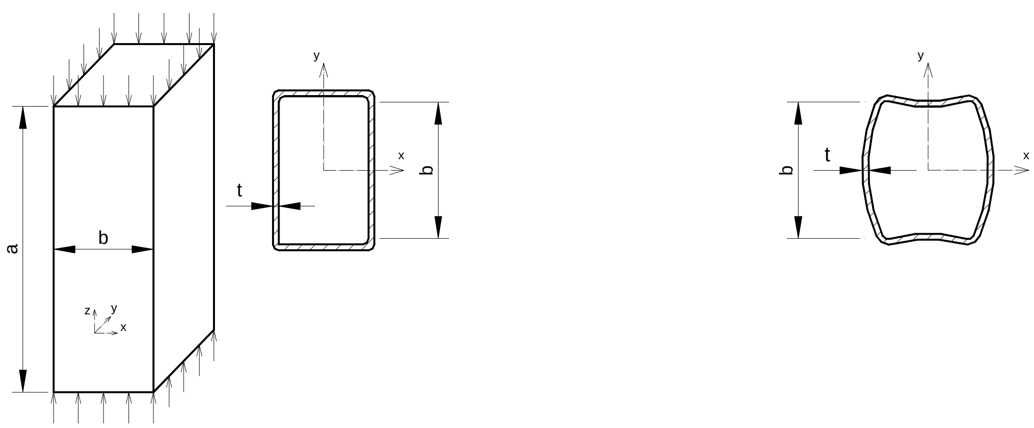

(a) The loading diagram and column section (b) The column section with the locally buckled walls

Fig. 3 A rectangular steel tube

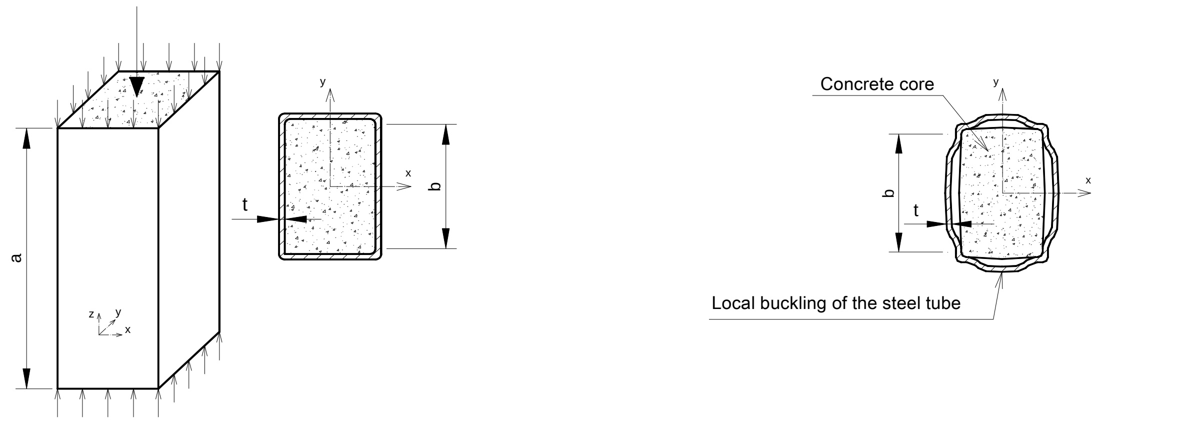

(a) The loading diagram and column section (b) The column section with the locally buckled steel shell

Fig. 4 A concrete-filled rectangular steel tube

Table 1 Correlation between the critical stress coefficient and the length-to-width ratio of a wall for m = 1

a/b	0.4	0.5	0.6	0.7	0.8	0.9	1.0
k_σ	9.44	7.69	7.05	7.00	7.29	7.83	7.69

$$w = A\sin\frac{m\pi x}{a}\left(C_1 e^{\alpha y} + C_2 e^{-\alpha y} + C_3\cos\beta y + C_4\sin\beta\right) \quad (16)$$

This particular solution (16) fulfils the boundary conditions on the transverse sides of the wall (Fig. 1) for $x = 0$ and $x = a$ and on the longitudinal sides for $y = 0$ and $y = b$ $\rightarrow w = 0$, and $\partial w/\partial y = 0$.

Having regarded the above mentioned boundary conditions, a transcendental Eq. (16) is obtained, and its solution provides the critical stress coefficient for various length-to-width ratios of a slender wall (Table 1).

3. Experiments on the analysed members

Based on the analysis presented above, steel sections RHS 200/100/3 made of Class S235 steel (Eurocode 3) and manufactured according to EN 10219-1(-2) were selected for the investigation of the local stability of CFSTs. Even though the sections employed were cold-formed and can be categorised as thin-walled members, the EN 1993-1-3 standard cannot be applied; instead, there is a stipulation that the EN 1993-1-1 standard must be applied. The concrete core in the composite members being analysed was made of Class C25/30 concrete (according to Eurocode 2). It can be stated that the presented section was selected in such a manner so as to fall outside the applicability of EN 1994-1-1 for its verification.

3.1 Material properties

A methodology and relevant procedures for the determination of material properties were based on the assessment of experimental results by reference to EN 1990. In principle, the adopted method involved using statistic methods for the assessment of the characteristic or design value of an independent property by introducing the corresponding quantile, while not only accounting for the variability of the results but also the number of experiments.

3.1.1 Material properties of the used steel

In order to specify the material properties of the steel used in experimental members, a tensile test was carried out. Thin-walled rectangular profiles, supplied by the selected manufacturer, were cut to produce elements for tensile test compliant with EN 10219-2. These were subsequently used for manufacturing 15 steel specimens to undergo the tensile test and tested according to the ISO 6892-1 standard requirements (see Fig. 5(a)). The resulting (average) "stress-strain" diagram that was used for the modelling of the members under observation is shown in Fig. 6. The results of the tensile test as well as the failure mode of the specimens are given in Table 2 and Fig. 5(b).

(a) The testing machine (b) Specimens after the tensile test

Fig. 5 A material test of the used steel

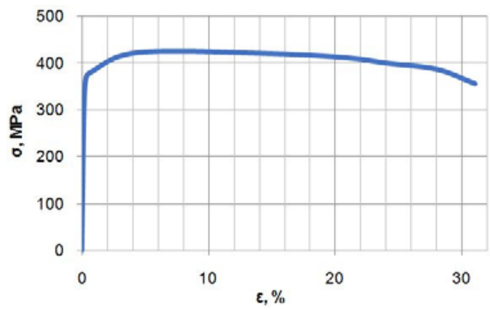

Fig. 6 The resulting σ-ε diagram of the used steel

Table 2 Results of a tensile test on the used steel

$f_{y0.2,m,}$ [MPa]	$f_{u,m,}$ [MPa]	E [GPA]	$f_{y,k,}$ [MPa] according to EN 1990	$f_{u,k,}$ [MPa] according to EN 1990
374.67	426.07	198.78	305.73	347.67

Table 3 Results of a material test of the used concrete

Day	Compressive strength of concrete		Bending tensile strength $f_{ct,fl}$, [MPa]	Secant modulus of elasticity E_{cm}, [GPa]	Density γ, [kg/m^3]
	Cylinder f_{ck} [MPa]	Cube $f_{ck,\ cube}$, [MPa]			
28	21.43	27.94	3.47	26.47	2269.52
150	25.83	33.53	4.07	28.50	2242.02

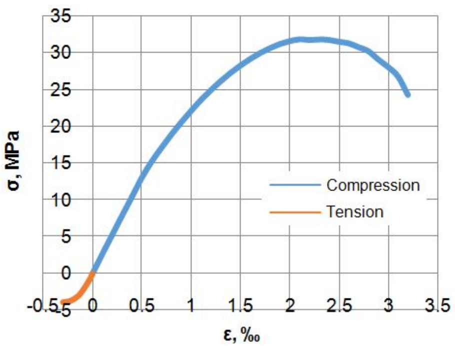

Fig. 7 The resulting σ-ε diagram of the used concrete

3.1.2 Material properties of the used steel

For the research in question, ready-mix concrete delivered fresh from the nearby mixing plant was used, C25/30 according to EN 206-1. The results of a material test of the used concrete are provided in Table 3 above.

All concrete specimens used in the material test mentioned above were designed, prepared and tested in compliance with the requirements provided in EN 12390-1(2). Mean values obtained from the experiments are listed in Table 3. Besides the values for the concrete at 28 days, values at the moment of the beginning of experiments on the analysed members were detected so that the current state of material properties of the concrete could be monitored. The resulting "stress-strain" diagram (Fig. 7) used for the modelling of these members in Section 4 could be drawn based on additional experimental measurements on prismatic specimens using strain gauges and inductive sensors to measure deformations (strain).

3.2 Material properties

Three types of short specimens without welded head plates and three types of short specimens with welded head plates were designed for the experimental purposes, each type 220/120/6 mm in size (Fig. 8). The total number of specimens was eighteen: six specimens of the first type of a hollow tube, six specimens of the second type of a concrete-filled tube, and six specimens of the third type of a concrete-filled tube loaded with a force applied on the steel section of the tube. Each specimen was milled out so that its end or head was level.

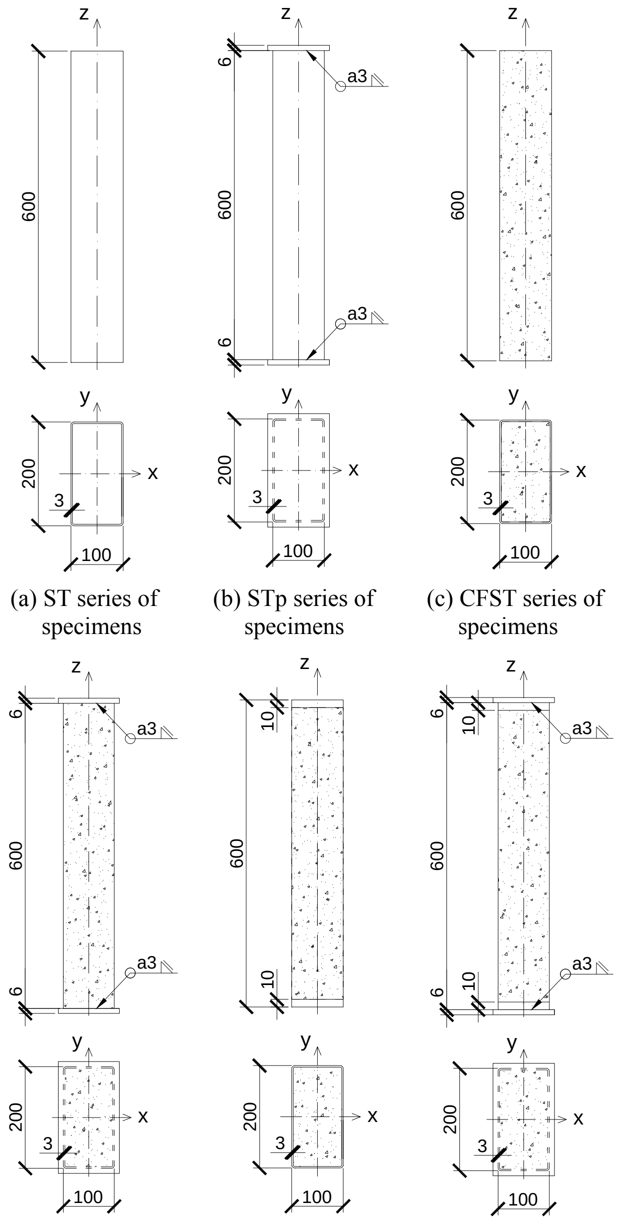

(a) ST series of specimens (b) STp series of specimens (c) CFST series of specimens

(d) CFSTp series of specimens (e) CFSTst series of specimens (f) CFSTstp series of specimens

Fig. 8 Types of specimens for experimental research

3.3 Experiments

Hollow experimental specimens without head plates were designated as ST-1, ST-2, and ST-3; those with head plates STp-1, STp-2, and STp-3. The specimens with concrete cores but without head plates were designated as CFST-1, CFST-2, and CFST-3; and those with both concrete fill and head plates as CFSTp-1, CFSTp-2, and CFSTp-3. The specimens with concrete cores, without head plates, and their steel elements of the composite sections acting in compression were designated as CFSTst-1, CFSTst-2,

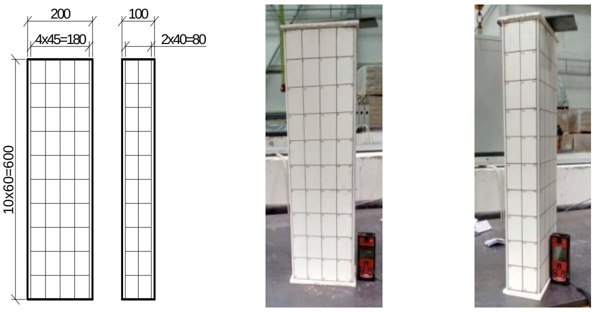

(a) Schematic diagram (b) Placement of a grid across the wide side of the section (c) Placement of a grid across the narrow side of the section

Fig. 9 A grid on the members being analysed

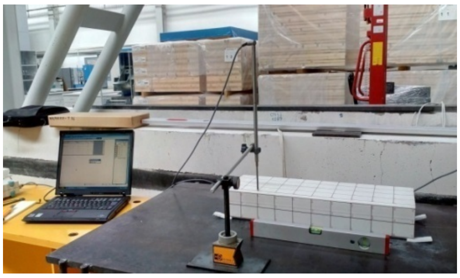

(a) Measurement of geometric imperfections

(b) Measurement of the width of walls in the short specimens

Fig. 10 Preparation of experiments

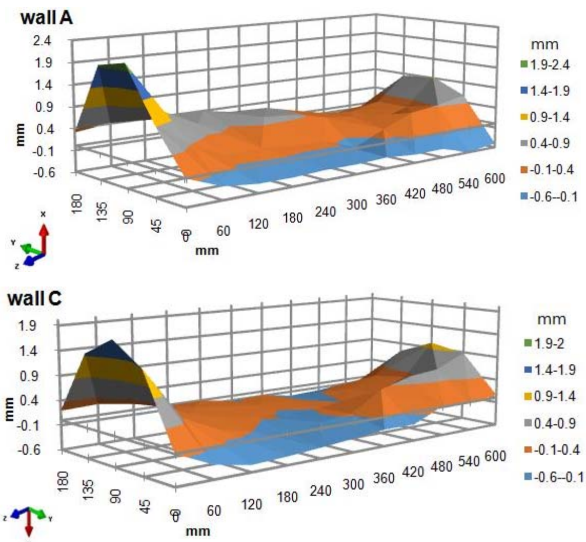

Fig. 11 Geometric imperfections of the wide walls of specimen ST-1

CFSTst-3, and finally, the identical ones with head plates as CFSTstp-1, CFSTstp-2, and CFSTstp-3.

For better clarity, easier identification of deformations and measurement of geometric imperfections, a grid was placed across each side of the composite member (see Figs. 9(a)-(c)). The geometric imperfections in the specimens were measured using an inductive sensor fastened in each point of intersection in the grid (Fig. 10(a)). The results of the measurements of imperfections of the one specimen from each type specimens are shown on Figs. 11-16. The basic geometry (thickness and lengths) of the investigated specimens of RHS 200×100×3 sections are shown in Table 4.

Load on the columns was exerted through a hinge in the upper part of the specimen. The hinge was created using a spherical component that was placed between the bearing plate at one end of the specimen and an M150 bolt that was

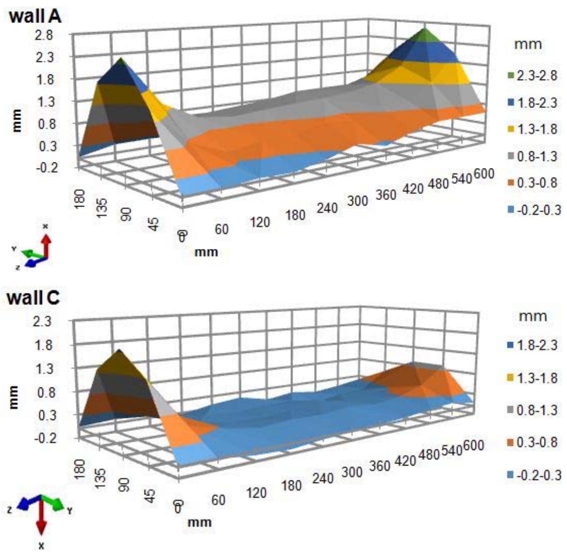

Fig. 12 Geometric imperfections of the wide walls of specimen STp-1d

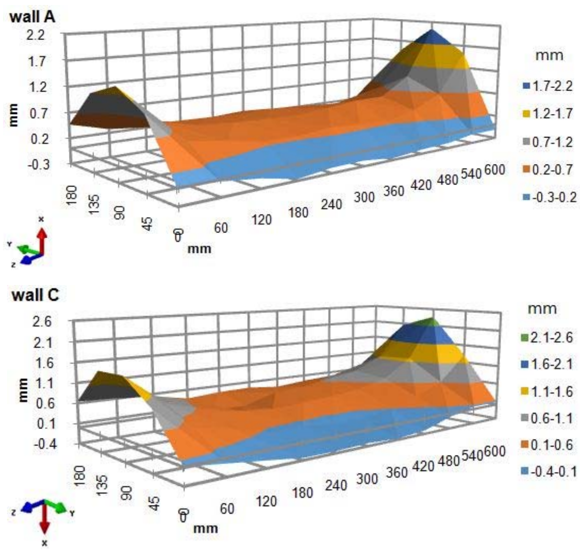

Fig. 13 Geometric imperfections of the wide walls of specimen CFST-1

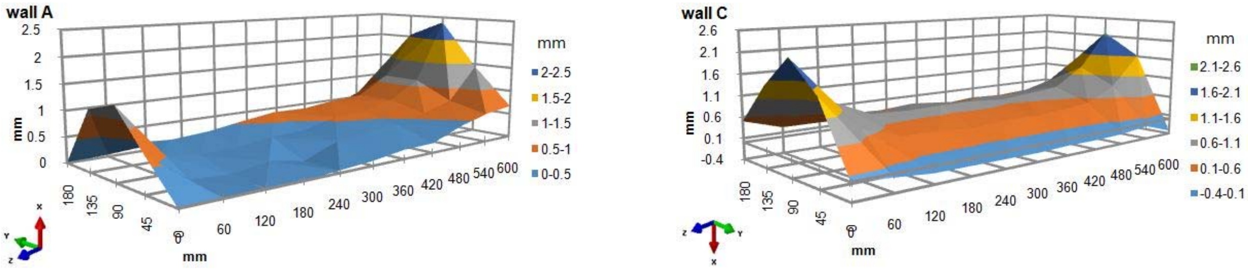

Fig. 14 Geometric imperfections of the wide walls of specimen CFSTp-1

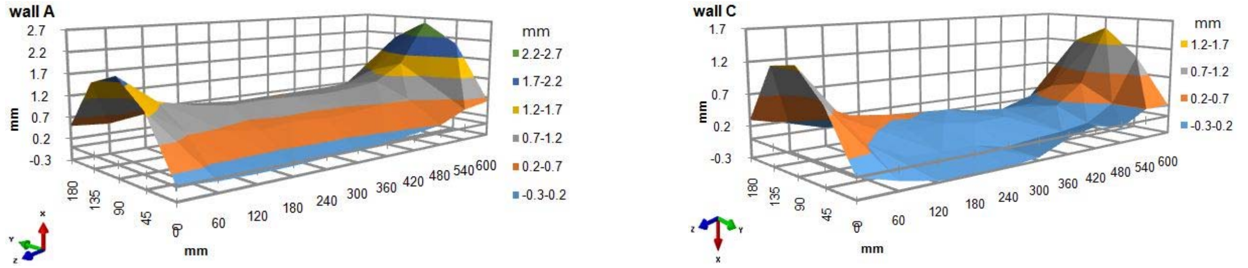

Fig. 15 Geometric imperfections of the wide walls of specimen CFSTst-1d

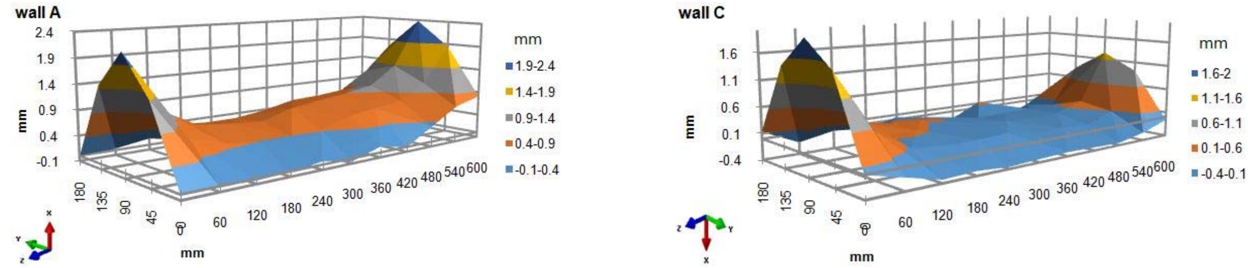

Fig. 16 Geometric imperfections of the wide walls of specimen CFSTstp-1

Table 4 Geometry of the short specimens

Specimen	Aver. thickness of the wall, [mm]	Aver. length of the column, [mm]
ST-1	2.75	599
ST-2	2.75	600
ST-3	2.77	600
STp-1	2.78	611
STp-2	2.78	613
STp-3	2.77	612
CFST-1	2.80	601
CFST-2	2.79	600
CFST-3	2.78	598
CFSTp-1	2.79	612
CFSTp-2	2.76	612
CFSTp-3	2.77	613
CFSTst-1	2.76	598
CFSTst-2	2.78	601
CFSTst-3	2.80	600
CFSTstp-1	2.79	612
CFSTstp-2	2.78	613
CFSTstp-3	2.80	612

driven into the loading gauge of the hydraulic press. The bearing plate was designed and constructed so as to allow centring the specimen using bolts in order to ensure the centric application of a compressive force.

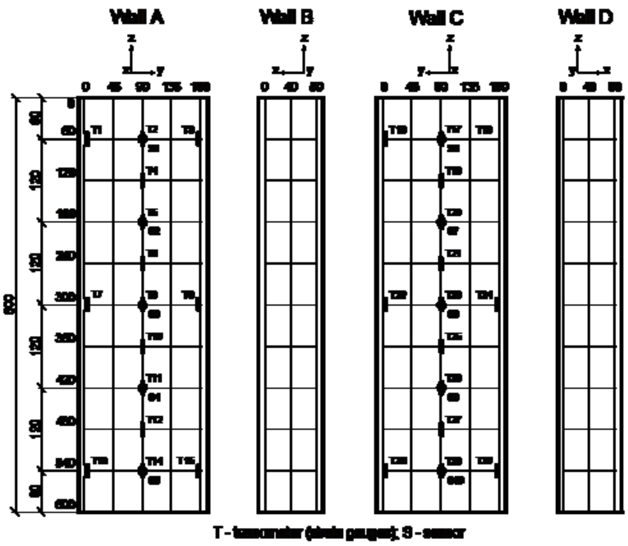

Fig. 17 Arrangement of strain gauges and inductive sensors on the experimental specimens

Table 6 Material properties of the steel in the FEM modelling

f_E, [MPa]	$f_{y0.2,m}$, [MPa]	$f_{u,m}$, [MPa]	E, [GPA]	Density γ, [kg/m^3]	Poisson's ratio v
236.57	374.67	426.07	198.78	7850	0.3

Deformations in the specimens were measured along the height of the wide sides of the analysed specimens by means of inductive sensors positioned in the mid-width of the wall. Stresses in the specimens in the longitudinal direction of the walls were measured using unidirectional strain gauges, bonded to the members as can be seen from Fig. 17. Loading steps were 20 kN, 50 kN and 25 kN for hollow tubes, concrete-filled tubes, and tubes partially filled with concrete, respectively. The amount of load decreased before the ultimate limit state was reached. In the course of application of the force into the specimens, the loading force was reduced twice to 5 kN, which was when approximately 25% and 50% of the assumed resistance was reached. The experimental results for the short specimens are given in Section 5.

4. Finite element method (FEM) modelling of the analysed members

Research work included the creation of a numerical behavioural simulation model for the short columns listed in the previous section, using the ABAQUS 6.13-4 computational-graphical software. The account was taken of the initial geometric imperfections in the modelling, which had been imported to ABAQUS by means of the CATIA V5-6 R2016 graphical software. The ABAQUS (SIMULIA 2013) library of structural elements was used, while the steel shell forming the composite section was created from the S4R-shell type of elements, and the concrete core from the solid C3D8R types, with the maximum size of finite elements of 15 mm (Figs. 20(a)-(c)) and the numbers of the elements given in Table 5. Loading of the columns was modelled according to the real course of loading during the experiments (Section 3): a uniformly applied short-term load through the plate of the hydraulic press until the ultimate limit state (ULS) was reached with double unloading at the stages with 25% and 50% of the ULS maximum. The load was applied to the composite columns by two possible modes: (a) concurrently to the rectangular steel tubular wall and the concrete fill (in CFST and CFSTp specimens); (b) only to the rectangular steel tubular wall (in CFSTst and CFSTstp specimens). The FEM computational analysis used "implicit" operations with a quasi-static application.

4.1 Material properties of the steel and concrete of the composite section in the FEM modelling

Material properties of the steel in the FEM modelling were taken from the material tests carried out on the real steel specimen (cf. Section 3.1.1), and they are shown in Table 6. The behaviour of the steel was simulated in

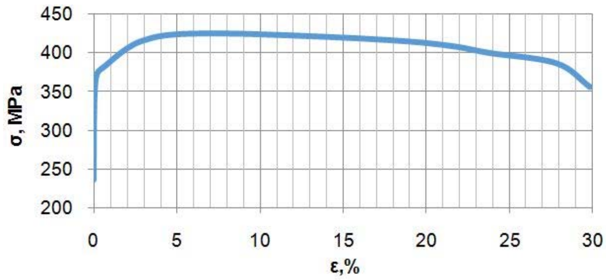

Fig. 18 Plastic region of the σ-ε diagram in modelling the steel using ABAQUS

accordance with the real resulting σ-ε diagram (Fig. 6), following the equations according to SIMULIA (2013) and describing the steel behaviour in the plastic region of the diagram after the limit of proportionality was reached (Fig. 18)

$$\sigma_{true} = \sigma_{nom}\left(1+\varepsilon_{nom}\right) \tag{17}$$

$$\varepsilon_{\ln}^{pl} = \ln\left(1+\varepsilon_{nom}\right) - \frac{\sigma_{true}}{E} \tag{18}$$

In modelling the concrete core of the composite section, the results of the material tests on the real concrete were used (cf. Section 3.1.2), which are given in Table 7. The behaviour of the concrete was simulated using the "Concrete damaged plasticity" model in ABAQUS, where, according to Drucker-Prager's theory of plasticity, the resulting "stress-strain" diagram was used (Fig. 7). Specific concrete properties for this theory were selected according to Hu *et al*. (2003), i.e., if the concrete core is situated inside the thin-walled steel shell, the force of confinement of the concrete is insignificant, and the following equations can be considered

$$f_{cc} = f_c + k_1 f_l \tag{19}$$

$$\varepsilon_{cc} = \varepsilon_c\left(1 + k_2\frac{f_l}{f_c}\right) \tag{20}$$

The expressions above describe the strength of concrete under various forces of confinement, considering the coefficients $k_1 = 4.1$ and $k_2 = 20.5$. If the slenderness ratio of the specimen walls is $h/t > 30$, the value $f_l = 0$. In the given model, the coefficient $k_3 = 0.5$ (see Fig. 19(a)). The resulting behavioural diagram for the confined concrete,

Table 7 Material test results for the concrete used in the FEM modelling

Compressive strength	Cylinder, [MPa]	25.83
	Prism, [MPa]	31.75
	Cube, [MPa]	33.53
Bending tensile strength, [MPa]		4.07
Poisson's ratio, v		0.2
Secant modulus of elasticity E_{cm}, [GPa]		28.50
Density γ, [kg/m^3]		2242.02

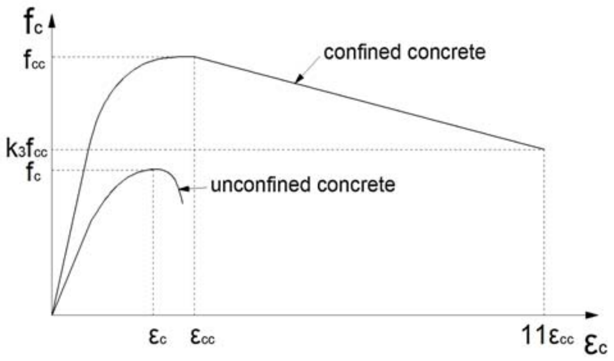

(a) Equivalent diagram for the confined concrete

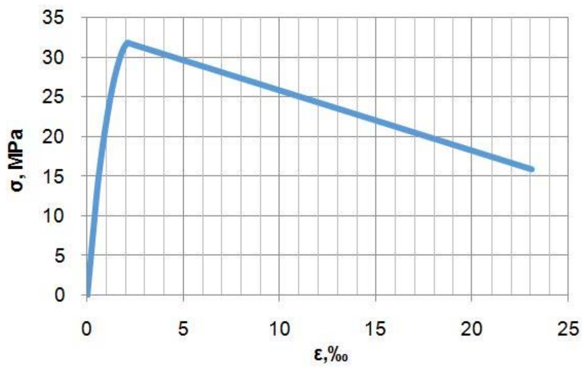

(b) Diagram for the concrete in the ABAQUS model

Fig. 19 The σ-ε curve for the concrete under compression

selected for the ABAQUS computations, is presented in Fig. 19(b).

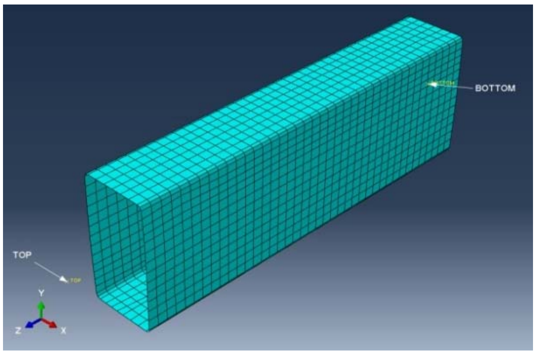

(a) ST and STp series

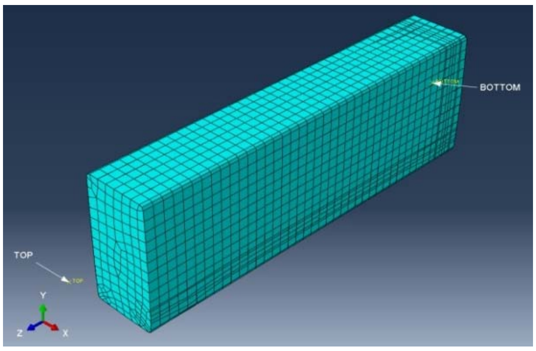

(b) CFST and CFSTp series

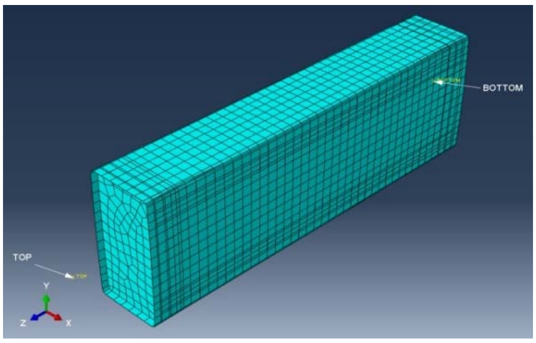

(c) CFSTst and CFSTstp series

Fig. 20 ABAQUS models of experimental specimens

4.2 Composite action between the steel and concrete elements of the composite section

The interaction between the steel and concrete elements of the composite section was modelled using two components: “normal”, i.e., the compression of the concrete core in the perpendicular direction on the steel shell walls, and “tangential”, i.e., the torsional resistance on the steel-concrete interface. In the ABAQUS modelling of the specimens, the tangential component was considered as friction between the concrete core and the steel shell in the composite section. As Rabbat and Russell (1985), Baltay and Gjelsvik (1990), and Evirgen and Tuncan (2014) suggested, the value of the friction coefficient may vary from quasi-zero up to 0.7. Qu *et al*. (2015) in their research has been proposed an empirical equation for predicting the average ultimate bond strength for rectangular hollow steel tubes filled with normal strength concrete. However, following Kanishchev and Kvocak (2015b), it can be stated that the influence of various values of the friction coefficient from within the above range is negligible if load is applied to the steel section only, or concurrently to both the steel section and concrete core of the composite member (see Figs. 8(c)-(f)). The influence of the friction coefficient is significant only if the load is directly applied to the concrete core, which is irrelevant for the research study in question. Therefore, in modelling the analysed composite columns, the friction coefficient was regarded by its average value of 0.3.

4.3 Boundary conditions for the analysed members

The boundary conditions corresponding to the real experiments were simulated in the computational-graphical ABAQUS software modelling of the behaviour of the composite columns being analysed. The simulation of the boundary conditions for the steel shell walls was in two variants: (a) hinged (pinned) ends (for ST, CFST, and CFSTst specimen types); and (b) fixed ends, simulated by the “fictitious” welding of the head plates at both ends of the tubes (for STp, CFSTp, and CFSTstp specimen types), i.e., rotation of the ends was prevented. In the ABAQUS environment, the end supports were modelled in “TOP” (the upper ends of the columns) and “BOTTOM” (the lower

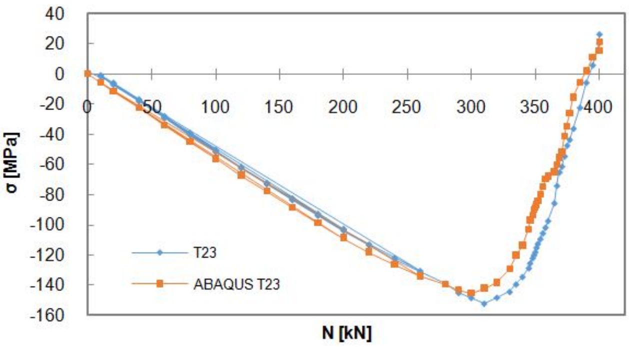

(a) Mid-wall stresses in Wall C

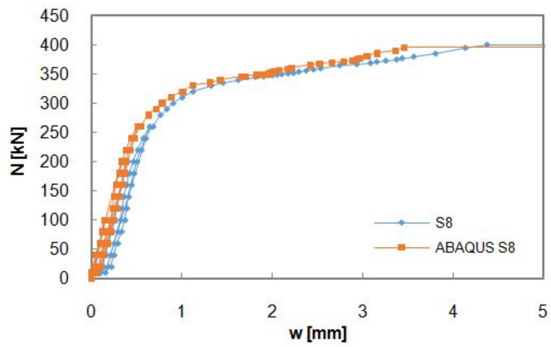

(b) Local buckling deformation of Wall C

Fig. 21 Comparison of experimental and ABAQUS modelling results in the ST-1 specimen

(a) Deformation of the specimen at failure

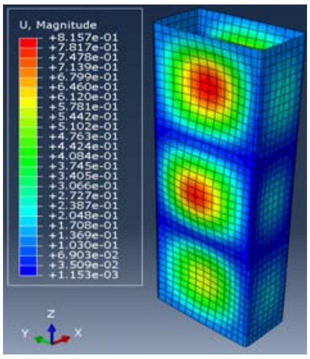

(b) Local buckling deformation of Walls C and D at σ_{cr}

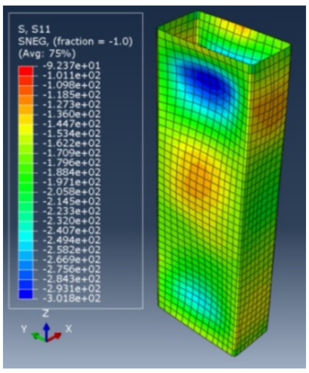

(c) Stresses in Walls C and D at N_{cr}

Fig. 22 Experimental and ABAQUS numerical modelling results for the ST-1 specimen

ends of the columns) reference points. Loading of the elements was through the upper “TOP” reference point, according to the real experimental conditions (see Figs. 20(a)-(c)). The reference points were joined as “rigid body constraint“ joints with the top and bottom edges of the steel shell in hollow tubular sections (ST and STp specimen types), or with the edges of the steel shell and the concrete core at both ends in the concrete-filled tubular sections (CFST and CFSTp specimen types).

5. Experimental results and results of ABAQUS numerical modelling of the analysed members

Mid-width critical stresses σ_{cr} in the wider walls of the sections were detected in the experiments by using strain gauges (Wall A and Wall C) due to a smaller flexural rigidity of these walls than that of the narrower walls (Wall

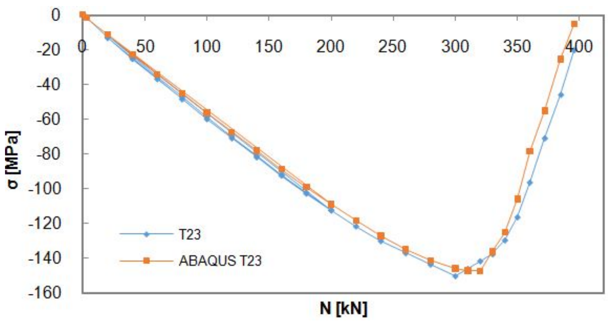

(a) Mid-wall stresses in Wall C

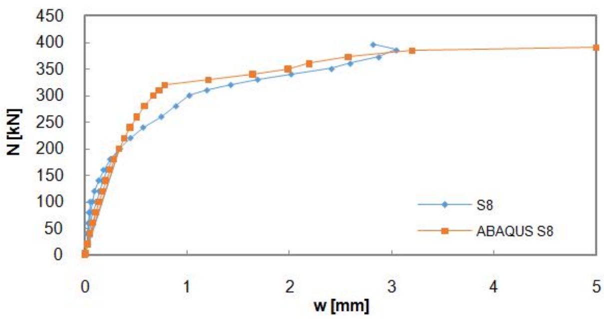

(b) Local buckling deformation of Wall C

Fig. 23 Comparison of experimental and ABAQUS modelling results in the STp-1 specimen

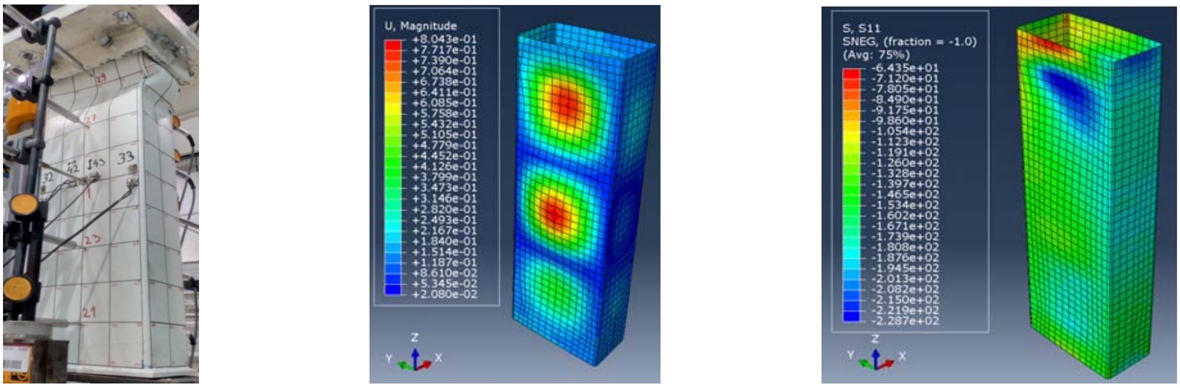

(a) Deformation of the specimen at failure (b) Local buckling deformation of Walls C and D at σ_{cr} (c) Stresses in Walls C and D at N_{cr}

Fig. 24 Experimental and ABAQUS numerical modelling results for the STp-1 specimen

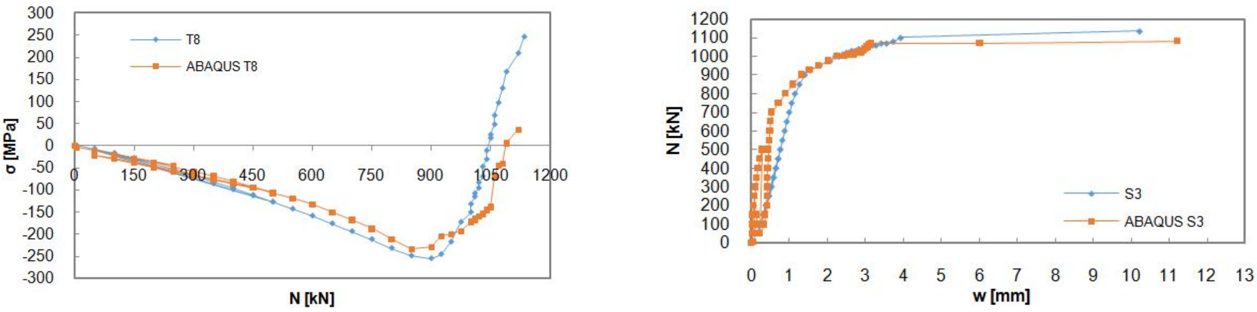

(a) Mid-wall stresses in Wall A (b) Local buckling deformation of Wall A

Fig. 25 Comparison of experimental and ABAQUS modelling results in the CFST-1 specimen

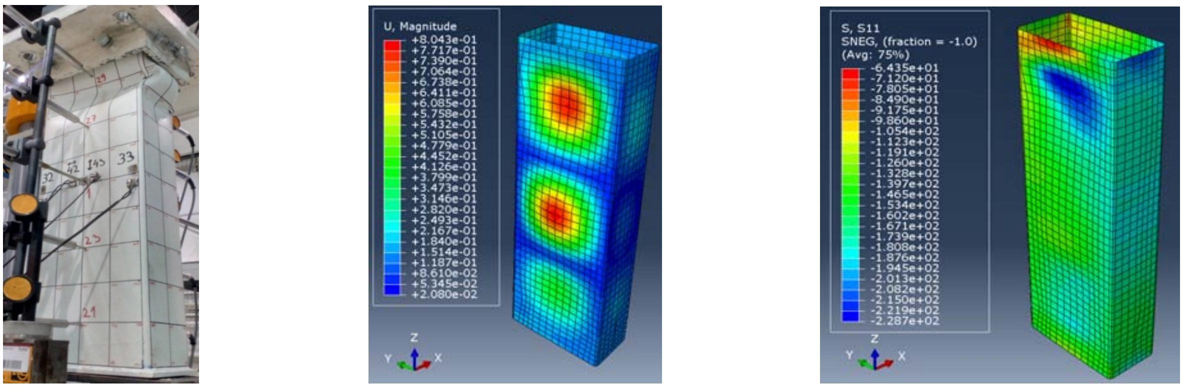

(a) Deformation of the specimen at failure (b) Local buckling deformation of Walls A and B at σ_{cr} (c) Stresses in Walls A and B before local buckling

Fig. 26 Experimental and ABAQUS numerical modelling results for the CFST-1 specimen

B and D) regarding the local loss of stability. The resulting critical stresses are shown in Table 9 in Section 6. The axial strength of the cross-section was also analysed during the experiments and modelling, as well as the wall deformations in locally buckled areas. As is shown in Figs. 21-24, the deformation of the local loss of stability in the hollow sections (the ST and STp series) is plotted as a sinusoid with three half-waves. In the concrete-filled specimens (the CFST, CFSTp, CFSTst, and CFSTstp series), the steel shell (tubular) walls buckle in a direction away from the composite section (see Figs. 25-32). In some

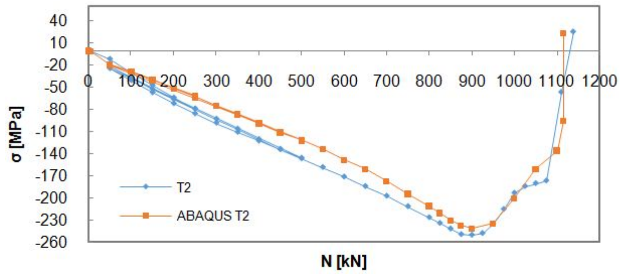

Fig. 27 Mid-wall stresses in Wall A of the CFSTp-1 specimen

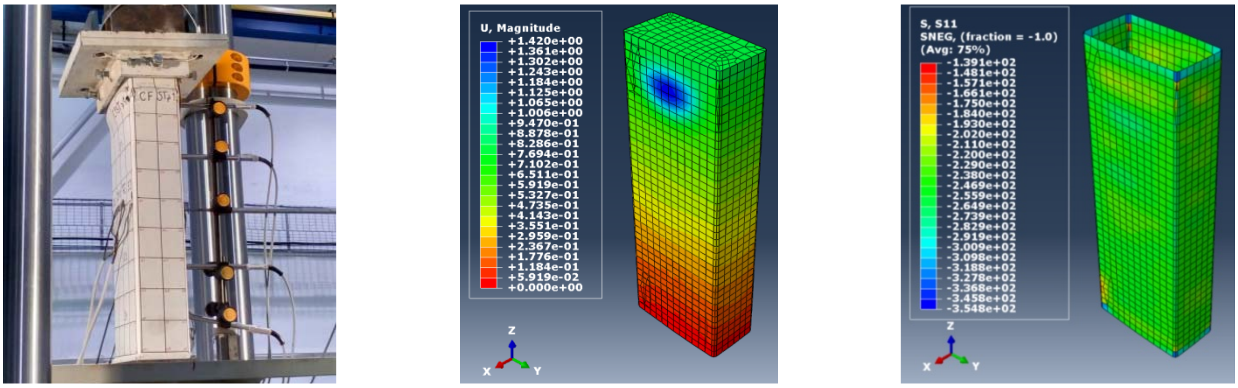

(a) Deformation of the specimen at failure (b) Local buckling deformation of Walls A and B at σ_{cr} (c) Stresses in Walls A and B before local buckling

Fig. 28 Experimental and ABAQUS numerical modelling results for the CFSTp-1 specimen

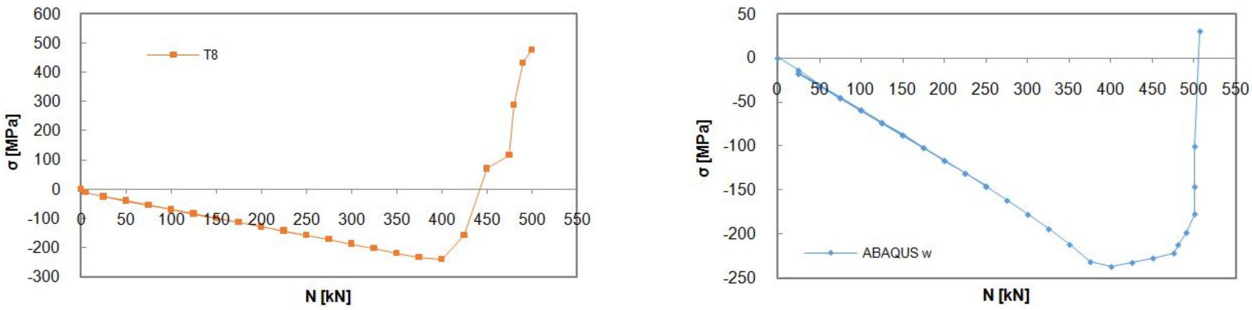

(a) Mid-wall stresses in Wall C (b) Mid-wall stresses in Wall C (ABAQUS)

Fig. 29 Comparison of experimental and ABAQUS modelling results in the CFSTst-1 specimen

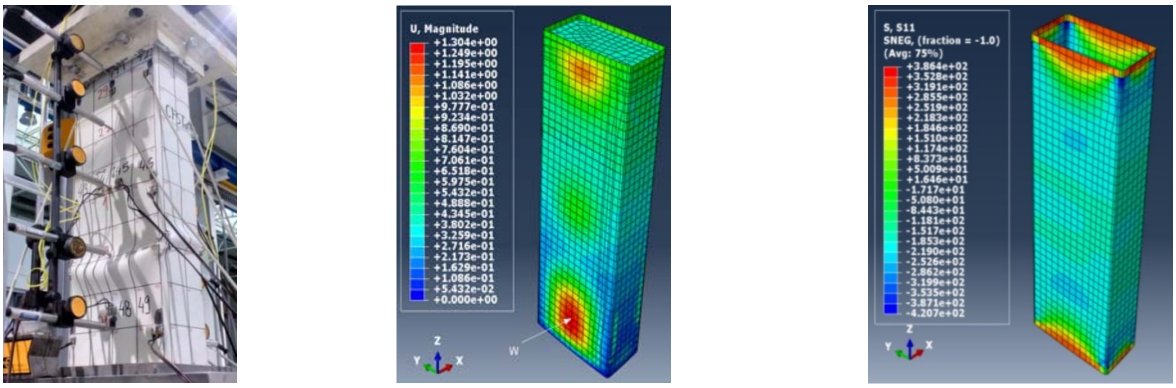

(a) Deformation of the specimen at failure (b) Local buckling deformation of Walls A and B at σ_{cr} (c) Stresses in Walls A and B before local buckling

Fig. 30 Experimental and ABAQUS numerical modelling results for the CFSTst-1 specimen

specimens in this series, local buckling deformations occurred outside the areas with the installed sensors, and it was impossible to take measurements.

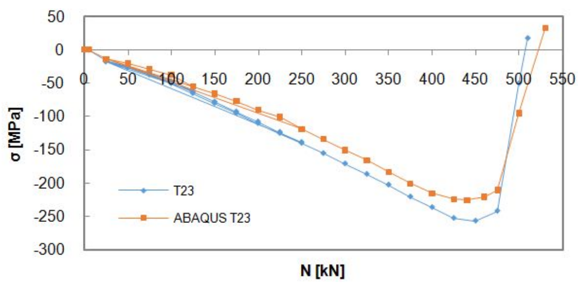

Fig. 31 Mid-wall stresses in Wall C of the CFSTstp-1 specimen

6. Analysis of the results

Based on both experimental measurements and numerical modelling of the short column specimens (Section 5) and the Eq. (14), the critical stress coefficients (k_{σ} for the hollow tubular sections and $k_{\sigma,comp}$ for the

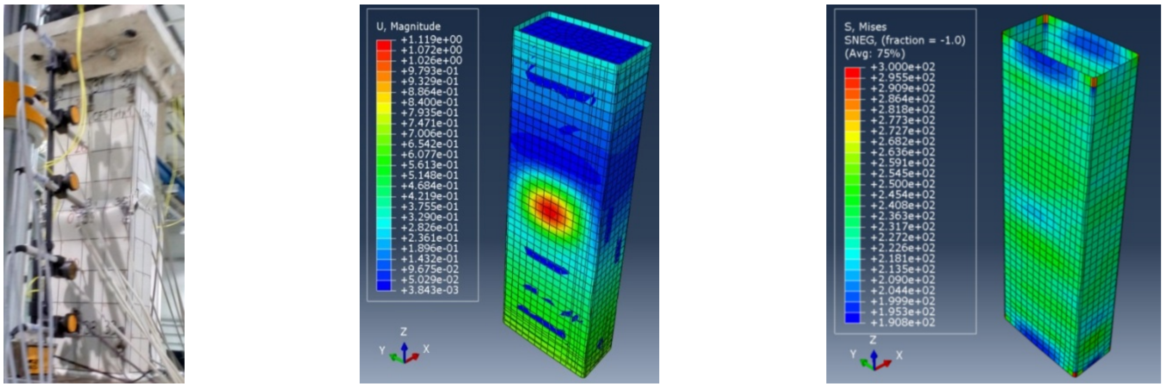

(a) Deformation of the specimen at failure (b) Local buckling deformation of Walls C and D at σ_{cr} (c) Stresses in Walls A and B before local buckling

Fig. 32 Experimental and ABAQUS numerical modelling results for the CFSTstp-1 specimen

Table 8 Analysis of the results in the analysed members

Specimen	Axial strength [kN]		Critical stress [MPa]		k_σ ($k_{\sigma,comp}$)			Difference k_σ ($k_{\sigma,comp}$) (Exp. vs ABAQUS) [%]
	Exp.	ABAQUS	Exp.	ABAQUS	Exp.	ABAQUS	EN 1993-1-5	
ST-1	310.15	300.05	152.07	145.30	4.11	3.93		4.42
ST-2	320.07	330.12	150.08	142.19	4.06	3.85		5.31
ST-3	310.15	320.10	159.94	145.28	4.33	3.93		9.23
STp-1	300.05	320.17	150.15	147.32	4.06	3.98	4.00	2.00
STp-2	300.25	300.56	153.30	140.14	4.15	3.80		8.43
STp-3	320.17	310.27	151.2	144.36	4.09	3.91		4.40
CFST-1	900.05	850.34	255.22	234.63	6.90	6.33		8.26
CFST-2	975.11	1025.34	275.77	237.02	7.46	6.41		14.07
CFST-3	1000.23	950.36	284.45	239.16	7.69	6.47		15.86
CFSTp-1	900.37	900.21	250.31	241.67	6.77	6.54	-	3.39
CFSTp-2	875	905.56	253.84	238.25	6.86	6.44		6.12
CFSTp-3	-	950.25	-	240.36	-	6.50		-
CFSTst-1	400.09	400.36	240.66	235.55	6.51	6.37		2.15
CFSTst-2	450.36	405.45	238.79	238.48	6.46	6.46		0.13
CFSTst-3	400.29	410.36	236.80	227.56	6.40	6.15		4.00
CFSTstp-1	450.07	440.15	257.02	225.17	6.95	6.10	-	12.23
CFSTstp-2	400.14	410.56	242.15	226.26	6.55	6.12		6.56
CFSTstp-3	450.10	425.36	250.74	228.36	6.78	6.18		8.95

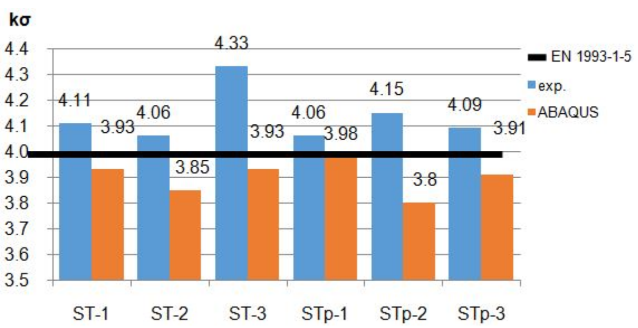

Fig. 33 Comparison of the critical stress coefficients for the ST(p) specimen series

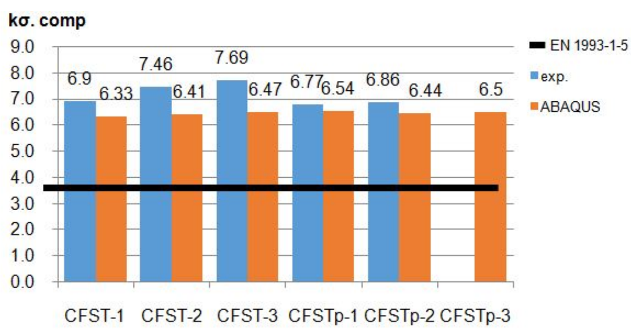

Fig. 34 Comparison of the critical stress coefficients for the CFST(p) specimen series

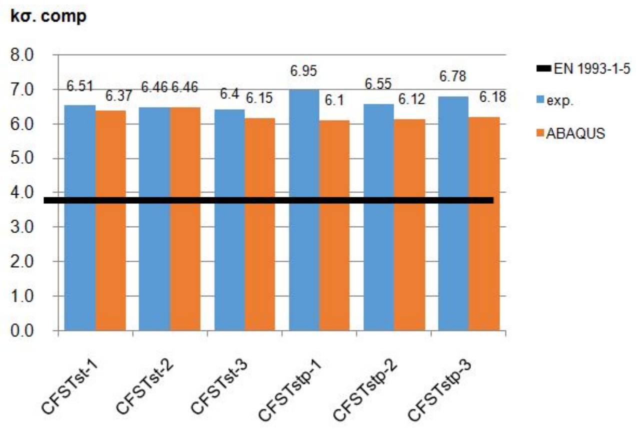

Fig. 35 Comparison of the critical stress coefficients for the CFSTst(p) specimen series

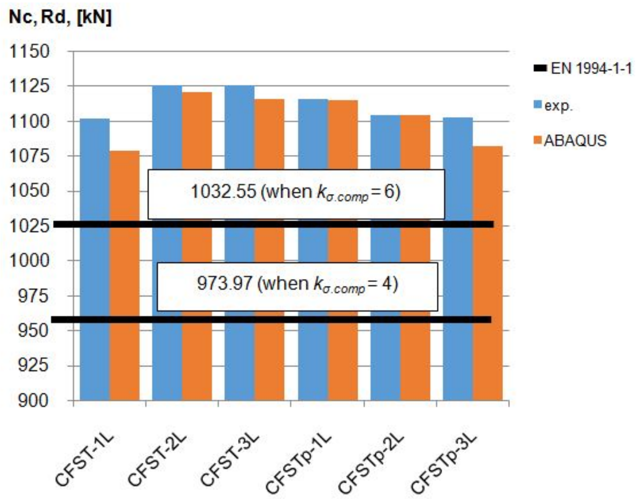

Fig. 36 Comparison of the axial strengths of the individual composite sections

concrete-filled tubular sections) were determined, as presented in Table 8.

The coefficients for the individual sections are further compared in Figs. 33-35. The comparison of the axial strength in the individual composite sections is provided in Fig. 36, where the values calculated compliant with Eurocode are also included, considering the critical stress coefficients for hollow sections, as well as the optimised values based on the research study mentioned above.

7. Conclusions

Based on the above theoretical, numerical and experimental analysis of the local stability of axially compressed rectangular thin-walled concrete-filled steel tubular sections, considering their initial geometric imperfections, it can be concluded that:

- The results of the research confirmed the feasibility and suitability of the application of rectangular Class 4 steel sections for composite members, which is currently unallowable according to EN 1994-1-1.
- Rectangular Class 4 steel sections (according to EN 1993-1-1) can also be employed for concrete-filled sections, while the design procedures stipulated in EN 1993-1-5 can be followed if the cross-sectional area of the steel element of the composite section is reduced by the critical stress coefficient. The fact was proved by both the numerical and experimental analyses in this paper, showing that the critical stresses remained elastic in all analysed specimens.
- In the composite section, i.e., the rectangular tube filled with concrete, the tubular walls are supported from the inside by the concrete core, which changes the boundary conditions for the walls (see Section 2).
- The experimental results and the results obtained from the used theoretical models correlate very well, which justifies the intention to investigate other types of composite members by theoretical modelling in the future (see Table 8).
- The minimum value of the critical stress coefficient in the CFST(p) members is 6.33 (the result of the CFST-1 specimen modelling), which is 9.6% smaller than its theoretical value (see Section 2.2). This phenomenon can be explained by the fact that the longitudinal edges of the real tubes are not perfectly fixed, and the concrete core contributes to the earlier local buckling of the walls.
- The minimum value of the critical stress coefficient in the CFSTst(p) members is 6.1 (the result of the CFSTst(p)-1 specimen modelling), which is also smaller by 12.9% than its theoretical value (see Section 2.2).
- The difference between the results obtained for the CFST(p) and CFSTst(p) specimens is negligibly small, and the application of the CFSTst(p)-type composite sections in construction practice does not serve any useful purpose since the resistance (load-bearing capacity) of the full (composite) section is not utilised (only that of the steel section).
- The welding of the head plates to the analysed members influenced only the shape and location of local deformations in the hollow and composite members.
- EN 1994-1-1 can be applied to the design of centrically compressed composite columns made of thin-walled concrete-filled steel sections, whereas local buckling is accounted for by calculating the effective cross-sectional area of the steel tubular section with the critical stress coefficient $k_{\sigma,comp} = 6$.
- For making broader conclusions, or complementary design proposals, it is necessary to carry out a higher number of experiments and numerically analyse the experiments, on whose ground it will be possible to optimise design calculations for such structures under a variety of axial force loading combinations (for example, eccentric load applications, a combination of compression and bending and many more).

Acknowledgments

The paper presented was supported by the projects: VEGA 1/0188/16 “Static and Fatigue Resistance of Joints and Members of Steel and Composite Structures” of the Scientific Grant Agency of the Ministry of Education, Science, Research and Sport of the Slovak Republic and the Slovak Academy of Sciences; ITMS: 26220220124 “Development of Bridges with Encased Beams of Modified Sections”; and the contract of the Slovak Research and Development Agency No. APVV-15-0486 “Analysis of Shear Connection Influence in Bridges with Encased Beams”.

References

Aslani, F., Uy, B., Tao, Z. and Mashiri, F. (2015), “Predicting the axial load capacity of high-strength concrete filled steel tubular columns”, *Steel Compos. Struct., Int. J.*, **19**(4), 967-993.

Aslani, F., Uy, B., Wang, Z. and Patel, V. (2016), “Confinement Models for High-Strength Short Square and Rectangular Concrete-Filled Steel Tubular Columns”, *Steel Compos. Struct., Int. J.*, **22**(5), 937-974.

Baltay, P. and Gjelsvik, A. (1990), “Coefficient of Friction for Steel on Concrete at High Normal Stress”, *J. Mater. Civil Eng., ASCE*, **2**, 46-49.

Bryan, G.H. (1891), “On the stability of a Plane Plate under Trusts in Its Own Plane, with Applications to the “Buckling” of the Sides of a Ship”, *Proceedings of the London Mathem. Soc.*, **22**, 54-67.

Chen, Z., Liu, X. and Zhou, W. (2018), “Residual bond behavior of high strength concrete-filled square steel tube after elevated temperatures”, *Steel Compos. Struct., Int. J.*, **27**(4), 509-523.

Ding, F., Fang, C., Bai, Y. and Gong, Y. (2014), “Mechanical Performance of Stirrup-Confined Concrete-Filled Steel Tubular Stub Columns under Axial Loading”, *J. Constr. Steel Res.*, **98**, 146-157.

Ding, F., Wen, B., Liu, X. and Wang, H. (2017), “Composite Action of Notched Circular CFT Stub Columns under Axial Compression”, *Steel Compos. Struct., Int. J.*, **24**(3), 309-322.

Ellobody, E. and Young, B. (2006), “Non-Linear Analysis of Concrete-Filled Steel SHS and RHS Columns”, *Thin-Wall. Struct.*, **44**, 919-930.

EN 10219-1 (2006), Cold-formed Welded Structural Hollow Sections of Non-Alloy and Fine Grain Steels, Part 1: Technical Delivery Conditions, European Committee for Standardization; Brussels, Belgium.

EN 10219-2 (2006), Cold-formed Welded Structural Hollow Sections of Non-Alloy and Fine Grain Steels, Part 2: Technical Delivery Conditions, European Committee for Standardization; Brussels, Belgium.

EN 12390-1 (2000), Testing Hardened Concrete - Part 1: Shape, Dimensions and Other Requirements for Specimens and Models, European Committee for Standardization; Brussels, Belgium.

EN 12390-2 (2000), Testing Hardened Concrete - Part 2: Making and Curing Specimens for Strength Tests, European Committee for Standardization; Brussels, Belgium.

EN 1990 (2011), Eurocode: Basis of Structural Design, European Committee for Standardization; Brussels, Belgium.

EN 1992-1-1, Eurocode 2 (2004): Design of Concrete Structures – Part 1-1: General Rules and Rules for Buildings, European Committee for Standardization; Brussels, Belgium.

EN 1993-1-1, Eurocode 3 (2005): Design of Concrete Structures – Part 1-1: General Rules and Rules for Buildings, European Committee for Standardization; Brussels, Belgium.

EN 1993-1-3, Eurocode 3 (2006): Design of Concrete Structures – Part 1-3: General Rules – Supplementary Rules for Cold-Formed Members and Sheeting, European Committee for Standardization; Brussels, Belgium.

EN 1993-1-5, Eurocode 3 (2006): Design of Concrete Structures – Part 1-5: Plated Structural Elements, European Committee for Standardization; Brussels, Belgium.

EN 1994-1-1, Eurocode 4 (2004): Design of Composite Steel and Concrete structures – Part 1-1: General Rules and Rules for Buildings, European Committee for Standardization; Brussels, Belgium.

Evirgen, B. and Tuncan, A. (2014), “Determination of Frictional Behaviour between Concrete and Steel Tube Interaction”, *7th Edition of the International European Conference on Steel and Composite Structures*, *EUROSTEEL 2014*, Naples, Italy, September.

Hu, H.-T., Huang, C.-S., Wu, M.-H. and Wu, Y.-M. (2003), “Non-Linear Analysis of Axially Loaded Concrete-Filled Tube Columns with Confinement Effect”, *J. Struct. Eng., ASCE*, **129**, 1322-1329.

Huang, Y., Long, Y. and Cai, J. (2008), “Ultimate Strength of Rectangular Concrete-Filled Steel Tubular (CFT) Stub Columns under Axial Compression”, *Steel Compos. Struct., Int. J.*, **8**(2), 115-128.

ISO 6892-1 (2016) Metallic Materials - Tensile Testing - Part 1: Method of Test at Room Temperature, The International Organization for Standardization; Geneva, Switzerlamd.

Kanishchev, R.A. (2016), “Analysis of Local Stability of Rectangular Tubes Filled with Concrete”, *Mag. Civil Eng.*, **64**(4), 59-68.

Kanishchev, R. and Kvocak, V. (2015a), “Effects of Stability on the Resistance of Composite Concrete-Filled Rectangular Steel Pipes According to World Standards”, *IABSE Conference: Elegance in Structures*, Nara, Japan, May.

Kanishchev, R. and Kvocak, V. (2015b), “Interaction of Steel and Concrete Elements in Rectangular Concrete-Filled Hollow Sections”, *Proceedings of the 7th International Scientific Conference on Civil and Environmental Engineering - Young Scientist 2015*, Kosice, Slovakia, April.

Lee, S. (2007), “Capacity and the Moment-Curvature Relationship of High-Strength Concrete-Filled Steel Tube Columns under Eccentric Loads”, *Steel Compos. Struct., Int. J.*, **7**(2), 135-160.

Lin, S.Q., Zhao, Y.G. and He, L.S. (2018), “Stress paths of confined concrete in axially loaded circular concrete-filled steel tube stub columns”, *Eng. Struct.*, **173**, 1019-1028.

Liu, D., Gho, W.M. and Yuan, J. (2003), “Ultimate Capacity of High-Strength Rectangular Concrete-Filled Steel Hollow Section Stub Columns”, *Constr. Steel Res.*, **59**(12), 1499-1515.

Lu, Z.-H., Zhao, Y.-G., Yu, Z.-W. and Chen, C. (2015), “Reliability-based assessment of American and European specifications for square CFT stub columns”, *Steel Compos. Struct., Int. J.*, **19**(4), 811-827.

Mouli, M. and Khelafi, H. (2007), “Strength of Short Composite Rectangular Hollow Section Columns Filled with Lightweight Aggregate Concrete”, *Eng. Struct.*, **29**, 1791-1797.

Patel, V.I., Liang, Q.Q. and Hadi, M. (2012), “Inelastic Stability Analysis of High-Strength Rectangular Concrete-Filled Steel Tubular Slender Beam-Columns”, *Interact. Multiscale Mech.*, **5**(2), 91-104.

Qu, X., Chen, Z., Nethercot, D.A., Gardner, L. and Theofanous, M. (2015), “Push-out tests and bond strength of rectangular CFST columns”, *Steel Compos. Struct., Int. J.*, **19**(1), 21-41.

Rabbat, B.G. and Russell, H.G. (1985), “Friction Coefficients of Steel on Concrete or Grout”, *J. Struct. Eng., ASCE*, **111**, 505-515.

Sakino, K., Nakahara, H., Morino, S. and Nishiyama, I. (2004), "Behavior of Centrally Loaded Concrete-Filled Steel-Tube Short Columns", *Struct. Eng., ASCE*, **130**(2), 180-188.

SIMULIA (2013), Abaqus 6.13. Analysis Users Guide, Volume I", Dassault Systems, RI, USA.

Storozhenko, L.I., Ermolenko, D.A. and Demchenko, O.V. (2014), "Rabota pod Nagruzkoi Szhatych Trubobetonnych Elementov s Usilennymi Jadrami", [The Work under Load of Compressed Concrete Pipe Elements with Reinforced Cores], Eff. of Resource Energy of Techn. in the Constr. Industry of Region, **4**, 288-292.

Timoshenko, S.P. (1971), Ustoychivost Sterzhney, Plastin i Obolochek [Stability of Rods, Plates and Shells], Nauka, Moskva, USSR.

Timoshenko, S. and Woinowsky-Krieger, S. (1959), *Theory of Plates and Shells*, McGraw-Hill Book Company, New York, NY, USA.

Uy, B. (2008), "Stability and Ductility of High-Performance Steel Sections with Concrete Infill", *J. Constr. Steel Res.*, **64**, 748-754.

Yang, Y. and Han L. (2009), "Experiments on Rectangular Concrete-Filled Steel Tubes Loaded Axially on a Partially Stressed Cross-Sectional Area", *J. Constr. Steel Res.*, **65**, 1617-1630.

Zhao, Y.G., Lin, S.Q., Lu, Z.H., Saito, T. and He, L.S. (2018), "Loading paths of confined concrete in circular concrete loaded CFT stub columns subjected to axial compression", *Eng. Struct.*, **156**, 21-31.

CC